

Ordering kinetics and steady state of self-propelled particles with random-bond disorder

Jay Prakash Singh^{1,*}, Sudipta Pattanayak^{2,†} and Shradha Mishra^{1‡}

¹*Department of Physics, Indian Institute of Technology (BHU), Varanasi, India 221005 and*

²*S. N. Bose National Centre for Basic Sciences,
J D Block, Sector III, Salt Lake City, Kolkata 700106*

(Dated: February 2, 2021)

In this study, we introduce a minimal model for a collection of polar self-propelled particles (SPPs) on a two-dimensional substrate where each particle has a different ability to interact with its neighbours. The SPPs interact through a short-range alignment interaction and interaction strength of each particle is obtained from a uniform distribution. Moreover, the volume exclusion among the SPPs is taken care of by introducing a repulsive interaction among them. We characterise the ordered steady state and kinetics of the system for different strengths of the disorder. We find that the presence of the disorder does not destroy the usual long-range ordering in the system. To our surprise, we note that the density clustering is enhanced in the presence of the disorder. Moreover, the disorder leads to the formation of a random network of different interaction strengths, which makes the alignment weaker and it results in the slower dynamics. Hence, the disorder leads to more cohesion among the particles. Furthermore, we note that the kinetics of the ordered state remains unaffected in the presence of the disorder. Size of orientationally ordered domains and density clusters grow with time with dynamic growth exponents $z_o \sim 2$ and $z_\rho \sim 4$, respectively.

I. INTRODUCTION

Collective behaviour of a large number of self-propelled particles (SPPs) or “flocking” is ubiquitous in nature. Examples of such systems range from a few micrometres, e.g., actin and tubulin filaments, molecular motors, epithelial cells [1–3], unicellular organisms such as amoebae and bacteria [4], to several metres, e.g., birds flock [5], fish school [6] and human crowd [7] *etc.* Interestingly, these systems show a collective motion on a scale much larger than each individual even in two dimensions, hence, long-range ordering (LRO) is observed. A minimal model was introduced by Vicsek *et al.* to understand the basic features of the collective behavior of self-propelled polar particles or “polar flock” [8]. In the last three decades, many variants of the Vicsek model are studied to understand various features of different model systems [18–21].

In these studies, authors mainly consider a collection of SPPs in a homogeneous system or medium. Recently, there is a growing interest to understand the effects and advantages of different kinds of inhomogeneities which are omnipresent in nature. Many studies show that the inhomogeneity can destroy the LRO present in a disorder-free system [22–30] whereas a few studies discuss special kinds of inhomogeneities which can enhance the ordering of a system [31, 32]. Therefore, the inhomogeneity can be useful for many practical applications, e.g., crowd control and faster evacuation *etc.*[33–37].

In the Vicsek model, each individual interacts through

a short-range alignment interaction and the strength of the interaction is the same for all the particles. But, in natural systems, each particle can have a different ability to influence its neighbors. However, scientists have not paid much attention to understand the effects of different interaction strengths in a polar flock. In a recent study, Bialek *et al.* show that pairwise inhomogeneous interactions between particles are sufficient to correctly predict the propagation of order throughout the entire flock [44].

In this work, we introduce a collection of polar SPPs with the random-bond disorder, and the particles interact through a short-range alignment interaction. Moreover, the volume exclusion among the particles is taken care of by introducing a repulsive interaction among them [11–13]. The strength of interaction for each particle is obtained from a uniform distribution between $[1 - \epsilon/2 : 1 + \epsilon/2]$, where ϵ is the strength of random-bond disorder. For $\epsilon = 0$, the model represents a disorder-free polar flock with uniform interaction strength for all the particles or the Vicsek-like model [8]. In this study, our focus is to understand the effects of the random-bond disorder on the true long-range ordered state in a disorder-free system [8, 14]. Also, we have characterised the effects of the random-bond disorder on the ordering kinetics of a polar flock.

We note that the presence of the disorder does not destroy the LRO present in a disorder-free system. However, the disorder affects the density clustering and results in more *cohesive* flocking. Furthermore, we also studied the ordering kinetics of the orientation and the density fields. When the system is quenched from an isotropic to an ordered steady state, both the orientation and the density fields coarsen with time. The size of the ordered orientation domains grows with time with an effective growth exponent $z_o \sim 2$ (same as for non-conserved model A [48, 49]). Also, the size of the

* jayps.rs.phy16@itbhu.ac.in

† sudipta.pattanayak@bose.res.in

‡ smishra.phy@iitbhu.ac.in

high-density domains grow with time with an exponent $z_\rho \sim 4$, similar to as found for a conserved field in active systems [50, 51].

The rest of the paper is organised as follows. In Sec.II, we discuss the model and simulation details. In Sec.III, the results from the numerical simulations are discussed. In Sec.IV, we conclude the paper with a summary and discussion of the results. Appendix A includes the details of linearised hydrodynamics to calculate the local density fluctuations in the system.

II. MODEL

We consider a collection of N polar self-propelled particles (SPPs) moving on a two-dimensional substrate. SPPs interact through a short-range alignment interaction within interaction radius R_I [8, 18, 19]. Moreover, the strength of interaction of each SPP is *different* unlike the Vicsek model of uniform interaction strength [8]. Furthermore, the volume exclusion among the particles is introduced through a soft repulsive binary force \mathbf{f}_{ij} , to avoid the clustering of particles to a single point for low noise or strong alignment [9]. Each SPP is defined by its position \mathbf{r}_i and orientation θ_i , and it moves along its direction vector $\mathbf{n}_i(t) = (\cos(\theta_i(t)), \sin(\theta_i(t)))$ with a fixed speed v_0 . The two update equations for the position $\mathbf{r}_i(t)$ and the direction vector $\mathbf{n}_i(t)$ are given by,

$$\mathbf{r}_i(t + \Delta t) = \mathbf{r}_i(t) + v_0 \mathbf{n}_i(t) \Delta t \quad (1)$$

$$\mathbf{n}_i(t + \Delta t) = \frac{\sum_{j \in R_I} J_j \mathbf{n}_j(t) - \beta \sum_{j \in R} \mathbf{f}_{ij} + \eta N_i(t) \xi_i(t)}{w_i(t)} \quad (2)$$

and soft repulsion force $\mathbf{f}_{ij} = \left(\exp \left[1 - \left(\frac{r_{ij}}{R} \right)^\gamma \right] - 1 \right) \mathbf{e}_{ij}$, where $\mathbf{f}_{ij} \neq 0$ if $r_{ij} < R$, and $\mathbf{f}_{ij} = 0$ if $r_{ij} \geq R$, where $R = R_I/10$ is the typical size of the particles. $r_{ij} = |\mathbf{r}_j - \mathbf{r}_i|$, $\mathbf{e}_{ij} = \frac{\mathbf{r}_{ij}}{r_{ij}}$ and the exponent $\gamma = 0.25$ is kept fixed such that the range of the repulsive force is smaller than the R_I .

Eq.((1)) represents the motion of the particle due to its self-propelled nature along the direction vector $\mathbf{n}_i(t)$ with a fixed speed v_0 . $\Delta t = 1.0$ is the unit time step. The first term on the right hand side in Eq.((2)) represents the short-range alignment interaction of the i^{th} particle with its neighbors within the interaction radius ($R_I = 1.0$), and J_j is the interaction strength of the j^{th} neighbor. The probability distribution of the interaction strength J , $P(J)$, is obtained from a uniform distribution of range $[1 - \frac{\epsilon}{2} : 1 + \frac{\epsilon}{2}]$ [46], where ϵ measures the degree of disorder. $\epsilon = 0$ corresponds to the uniform interaction strength ($J_i = 1$ for all the particles) like the Vicsek model [8] whereas $\epsilon = 2$ corresponds to the maximum disorder in the system. The second term indicates the soft-repulsive force due to the finite size of the particles. The strength of the force β is kept fixed to 0.01.

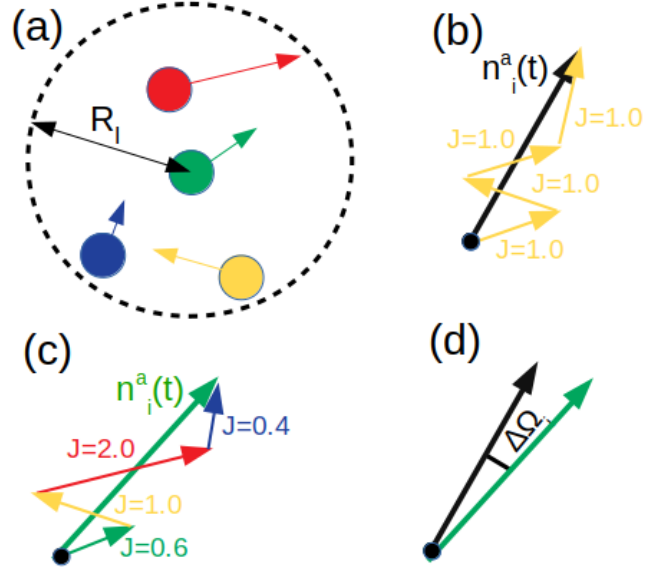


FIG. 1. (color online) (a) Cartoon picture of the model. The dashed circle of radius R_I represents the interaction radius of the green tagged particle of radius R (at the centre). The circles of various colors of radius R indicate the neighbors of the tagged particle. The arrows of different lengths represent the interaction strength J 's of the respective particle. (b,c) The cartoon picture of the resultant direction of the tagged particle due to the alignment interaction with its neighbors for the uniform strength (clean polar flock) and the varying (RBDPF) interaction strength model, respectively. Black and green arrow represent the resultant directions of the tagged particle in (b) and (c), respectively. (d) The relative difference in the resultant direction $\Delta\Omega_i$ of the tagged particle for the clean and the RBDPF.

Furthermore, the third term in the Eq.((2)) denotes the vector noise which measures the error made by the particle while following its neighbors. $\xi_i(t)$ is a random unit vector and $N_i(t)$ denotes the number of neighbors within the interaction radius of the i^{th} particle at time t . η represents the strength of the noise and it can vary from 0 to 1. $w_i(t)$ is the normalisation factor, which reduces the R. H. S. of the Eq.((2)) to a unit vector.

The cartoon picture of the model is shown in Fig.1 (a). The resultant direction vector $\mathbf{n}_i^a(t)$ of the i^{th} particle (due to alignment interaction with its neighbors) for the disorder-free ($\epsilon = 0$) and the maximum disorder ($\epsilon = 2.0$) system are shown in Fig.1(b) and (c), respectively. In Fig.1(d), $\Delta\Omega_i$ represents the difference in the resultant vectors shown in Fig. 1(b) and (c). For a disorder system the resultant direction vector is closer to the particle's original direction, which is due to the weaker alignment in the presence of disorder. In analogy with the equilibrium random-bond XY (RBXY)-model [45, 46], we name our model as random-bond disorder in polar flock (RBDPF). However, for $\epsilon = 0$, the model reduces to a disorder-free or *clean* polar flock. We numerically update the Eqs.((1)) and ((2)) for all SPPs sequentially. One simulation step is counted after the update of Eqs.((1)) and ((2)) once for all the particles.

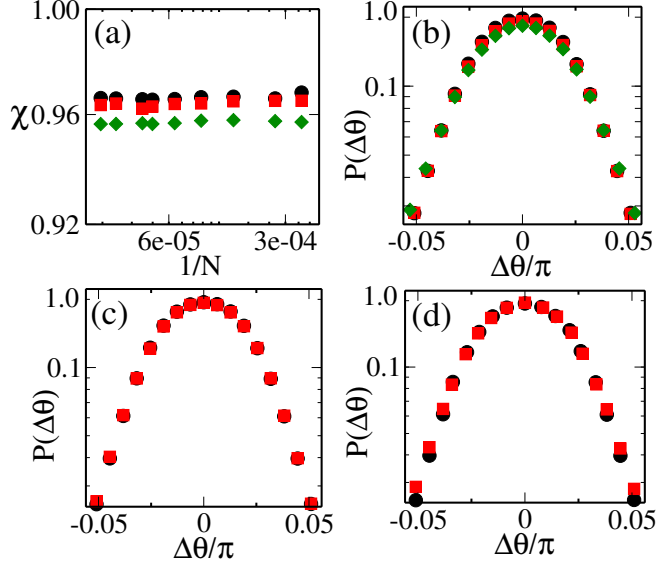


FIG. 2. (color online) (a) Plot of the global orientation order parameter χ vs. $1/N$ for different ϵ in semi-log X scale. (b) Probability distribution function of the mean orientation fluctuation $P(\Delta\theta)$ vs. $\frac{\Delta\theta}{\pi}$ for different ϵ in semi-log Y scale. $N = 62500$. The filled black circles, red squares, green diamonds represent data for $\epsilon = 0.0, 1.0$, and 2.0 , respectively. (c,d) Plots of $P(\Delta\theta)$ vs. $\frac{\Delta\theta}{\pi}$ for different system sizes for $\epsilon = 0.0$ and $\epsilon = 2.0$ in semi-log Y scale, respectively. The filled black circles and red squares denote $N = 40000$ and 62500 , respectively.

Periodic boundary conditions (PBC) are used for a system of size $L \times L$, and L is varied from 50 to 512 (N from 2500 to 262144). The number density of the system is defined as $\rho_0 = \frac{N}{L \times L}$. Most of the results are obtained for density $\rho_0 = 1.0$ and some results are calculated for $\rho_0 = 0.5$ and 2.0 . The self-propulsion speed is fixed at $v_0 = 0.5$. The noise strength η is fixed at $\eta = 0.2$, such that the steady state is an ordered state and the system is away from the order-disorder phase transition [19]. The effect of random bond disorder on the system near order-disorder phase transition will be our future study [10]. We study the properties of steady state as well as the ordering kinetics of the orientation and density fields for different strengths of the disorder ϵ . We consider time up to 10^4 to study the ordering kinetics and steady state results are obtained from time up to 10^6 and 20 independent realizations are used for the better statistics of the numerical results.

III. RESULTS

A. Steady-state behaviour

In uniform-interaction strength models or Vicsek-like models [8, 18, 19], the ordered state exhibits a true long-range order in two dimensions. In general, the orientation ordering in the system is characterised by the

global orientation order parameter, which is defined as³ $\chi(t) = \frac{1}{N} |\sum_{i=1}^N \mathbf{n}_i(t)|$. $\chi(t)$ is very small and it is of the order $\frac{1}{\sqrt{N}}$ for the disordered state and it is close to unity in the ordered state. The variation of the mean value of $\chi(t)$, χ , vs. $1/N$ for different ϵ is shown in Fig.2(a), where “mean” is obtained from the value of $\chi(t)$ in the steady state and it is averaged over 20 independent realisations. We note that χ is independent of system size for different strengths (ϵ) of the disorder. However, the magnitude of χ shows a small variation on increasing the strength ϵ of the disorder. Furthermore, the probability distribution function (PDF) of fluctuation from the mean orientation of the particles $P(\Delta\theta)$ is shown for different values of ϵ in Fig.2(b), where $\Delta\theta = \theta_i - \bar{\theta}$ where, θ_i is the orientation of i^{th} particle and $\bar{\theta}$ is mean orientation of the flock. The peak of the PDF decreases with the increasing disorder strength ϵ . Moreover, the change is small but it is consistent with increasing ϵ . To confirm the long-range ordering, we plot $P(\Delta\theta)$ for different system sizes for $\epsilon = 0$ and 2 , in Fig.2(c) and (d), respectively. $P(\Delta\theta)$ distribution for different system sizes overlaps on each other for a particular ϵ . Therefore, the magnitude of the global ordering shows a small decay with increasing ϵ but the ordered steady state remains long range for all ϵ of RBDPF.

Behaviour of the flock state

As discussed in the previous paragraph, the disorder does not affect the usual long-range ordering in the system. Furthermore, we study the effect of the disorder on the clustering of particles in the steady state. The snapshots of the system for three different strengths of the disorder, $\epsilon = 0, 1$ and 2 at different times are shown in Fig.3. At late time, we note that the number of particles inside a unit sized cell increases for high disorder strength, as shown in Fig.3. Hence, the particles cluster more cohesively for high disorder strength ϵ . To further characterise the density clustering, we calculate the probability distribution function (PDF) $P(n, \epsilon)$ of the number of particles (n) inside the interaction radius for different ϵ . $P(n, \epsilon)$ for different ϵ decay with an exponential tail, $P(n, \epsilon) \sim P_o(\epsilon) \exp(-n/n_c(\epsilon))$ where n_c is a constant and it is obtained from the exponential fitting, as shown in Fig.4(a). The distribution flattens with the increasing strength of the disorder. Therefore, the particles are having more number of neighbors inside its interaction radius, i.e. more compact/dense clustering in the system. In the inset of Fig.4(a), the variation of $P(n)$ with ‘n’ is shown. We note that the peak of the distribution decreases with the disorder strength. It further confirms that the probability of the small clusters is less for high disorder strengths. In the Fig.4(b), the scaling plot of $P(n, \epsilon)/P_o(\epsilon)$ vs. $n/n_c(\epsilon)$ is shown for different ϵ . We note that n_c increases linearly with the disorder strength ϵ , as shown in the inset of Fig.4(b). It also suggests that the number of neighbors for each particle is increasing

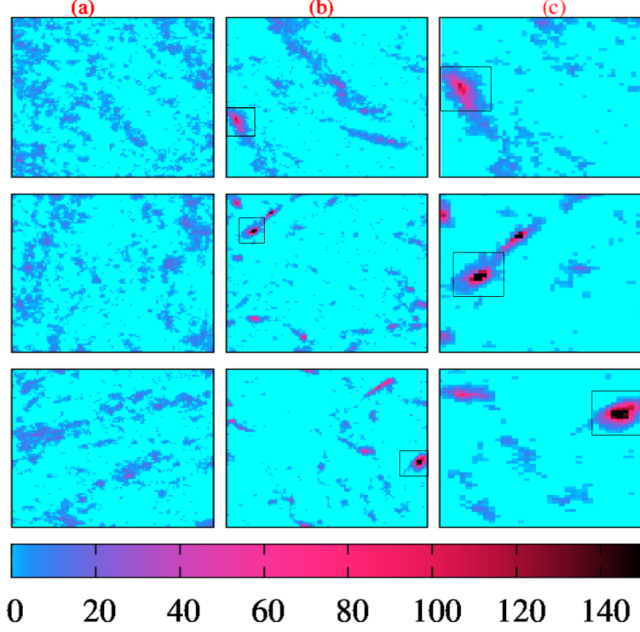


FIG. 3. (color online) Horizontal panel: top to bottom panels are real space snapshots of the local number density of the SPPs for different ϵ at different times t . The topmost panel is for $\epsilon = 0$, middle one is for $\epsilon = 1$ and bottom is for $\epsilon = 2$. Vertical panels: from left to right, (a) to (c), are real snapshots of the local number density of the SPPs at different time t for each ϵ . Leftmost panel (a) is for $t = 5,000$, the middle one (b) is for $t = 45,000$ and (c) represent zoomed snapshots of (b) at time $t=45000$. The square boxes in (c) represent the zoomed version of the square boxes of (b). $N = 10,000$. The color bar represents the local number density of the particles. .

with ϵ . Therefore, the scaling behavior of the PDFs confirm that the clusters are statistically identical for different strengths ϵ of the disorder. To further understand the density clustering, we calculate the local density fluctuation, $\delta\phi(\epsilon) = \sqrt{\frac{1}{L^2} \sum_{j=1}^{L^2} (\phi_j(\epsilon))^2 - (\frac{1}{L^2} \sum_{j=1}^{L^2} \phi_j(\epsilon))^2}$, for different ϵ . To calculate $\delta\phi(\epsilon)$, we divide the full $L \times L$ system into L^2 number of unit sized sub-cells. $\phi_j(\epsilon)$ is the number of particles in the j^{th} unit sized sub-cell and $\delta\phi(\epsilon)$ is the measure of the standard deviation in number of particles in a unit sized sub-cell of the system. Furthermore, we define the relative density phase separation by $\Delta\Phi(\epsilon) = \delta\phi(\epsilon) - \delta\phi(0)$, where $\delta\phi(0)$ is the local density fluctuation for the clean system ($\epsilon = 0$).

The plot of $\Delta\Phi(\epsilon)$ vs. ϵ for three different densities $\rho_0 = 0.5, 1.0$ and 2.0 is shown in Fig.4(c). We note that the density clustering increases with ϵ for all the densities. We also calculate the magnitude of the density fluctuation using linearized hydrodynamic equations of motion for the coarse-grained density and orientation fields of the system. The dashed lines in Fig.4(c) is obtained from the linearized hydrodynamics in Eq.(A21). Since the linearized hydrodynamic works well in the mean field limit, hence, the data matches well for lower density and deviates for the higher densities. The details of

the hydrodynamic calculation are given in Appendix A⁴. Therefore, the random-bond disorder which has a tendency to disturb the ordering in the corresponding equilibrium system [46, 47], enhances the density clustering in RBDPF. Hence, the disorder introduces more *cohesion* among the SPPs.

Furthermore, we calculate the global number fluctuation in different sub-systems, $\Delta\mathcal{N} = \sqrt{\langle N^2 \rangle - \langle N \rangle^2}$, N , N^2 , and $\Delta\mathcal{N}$ represent the number of particle in a box of size l , the square of the number of particles in a box of size l and standard deviation, respectively. We varied l from 1 to the 1/4 of the system size. $\langle \rangle$ represents the average over many snapshots and many ensembles. We show the plot of $\Delta\mathcal{N}$ vs. the mean number of particles in the sub-system $\langle N \rangle$ for different ϵ in Fig.4 (d). Although the disorder enhances the local density clustering, $\Delta\mathcal{N}$ remains unaffected in the presence of the disorder and the system shows the usual Giant number fluctuation for all ϵ . Also, we note that $\Delta\mathcal{N} \simeq \langle N \rangle^{1.6}$, and it matches well with the previous studies of polar self-propelled particles interact through the Vicsek type interaction [18, 19, 52].

Distribution of particles in flock

In the previous section, we note that the random-bond disorder introduces more cohesion among the SPPs. To understand this mechanism of cohesion for higher disorder, we analyse a cluster and study the distribution of particles inside it, as shown in Fig.5. The snapshot of particles' position inside the interaction radius of a tagged particle is shown in Fig.5(a). We divide the full range of $J \in [0, 2]$ (for maximum disorder $\epsilon = 2$) in four parts $J(1) \in [0 : 0.5]$, $J(2) \in [0.5, 1.0]$, $J(3) \in [1.0 : 1.5]$ and $J(4) \in [1.5 : 2.0]$ and they are shown by different colors. The snapshot shows that the particles of different interaction strengths are distributed homogeneously inside an interaction radius of a given particle. Furthermore, we calculate the probability distribution function (PDF) $P(n_{J(i)})$ of the particles $n_{J(i)}$ of the four different ranges of $J(i)$, where $i = 1, 2, 3, 4$, as shown in Fig5(b). We note that $P(n_{J(i)})$ for each range of $J(i)$ are nearly identical and it confirms that particles are distributed homogeneously in the system. We also plot the particles orientation distribution $P(\Delta\theta_{J(i)})$ for the four different ranges of $J(i)$. The orientation distribution of the particles of different ranges, $P(\Delta\theta_{J(i)})$, remains unchanged, as shown in the Fig.5(c). Hence, the clusters are a homogeneous network of particles of different interaction strengths for the RBDPF. Therefore, a moving particle always experiences a random network of interaction strengths during its motion. The resulting orientation due to the random strength of neighbours results in the weaker alignment, hence, the system has less ordering. Furthermore, we calculate the effective transport speed $v(\epsilon, t)$ of the particles for different strengths of the disorder. The mean displacement of the particles is calculated by taking the square root of their

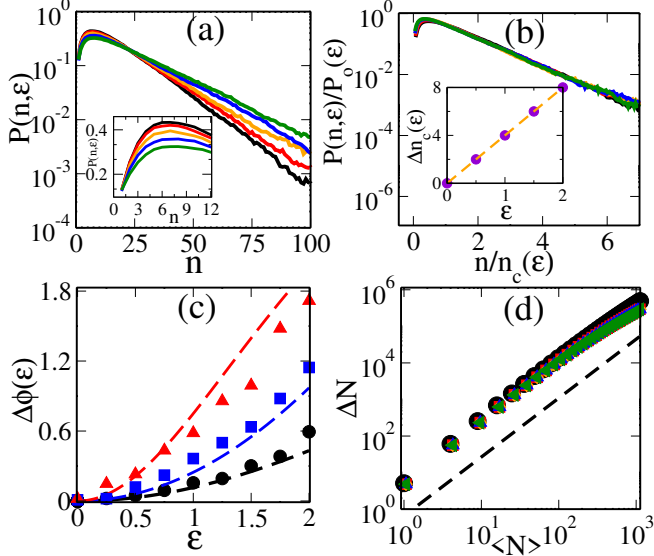


FIG. 4. (color online) (a,b) Plots of $P(n, \epsilon)$ vs. n and $P(n, \epsilon)/P_o(\epsilon)$ vs. n/n_c in semi-log Y scale for different ϵ , respectively. The black, red, orange, blue and green lines represent $\epsilon = 0.0, 0.5, 1.0, 1.5$, and 2.0 , respectively. Inset of (a) is zoomed near to the peak of the distribution of main plot. $N = 62500$. In the inset of (b) Plot of $\Delta n_c(\epsilon) = n_c(\epsilon) - n_c(0)$ vs. ϵ . Voilet circles represent the data obtained from the fitting function $\exp(-n/n_c(\epsilon))$ and orange dashed line indicates the linear variation. (c) Variation of local density fluctuation $\Delta\Phi(\epsilon)$ with ϵ . The filled black circles, blue squares and red triangles represent the numerical data points for $\rho_0 = 0.5, 1$ and 2 , respectively. Error bars are in the order of symbol sizes. $N = 62500$. The black ($\rho_0 = 0.5$), red ($\rho_0 = 1.0$) and blue ($\rho_0 = 2.0$) dashed line indicate the variation of $\Delta\Phi(\epsilon)$ obtained from the analytical calculations, as shown in Appendix.A in Eq.(A21). (d) Plot of the global number fluctuation (ΔN) vs. the mean number of particles ($\langle N \rangle$) in log-log scale. $N = 62500$. The dashed line represents slope = 1.6.

mean square displacement, $\Delta r(t) = \sqrt{\langle \Delta^2 r(t) \rangle}$ where $\Delta^2 r(t) = \sum_i^N (\langle r_i^2(t) \rangle - \langle r_i(t) \rangle^2)$. Moreover, the transport speed of the particles is defined as $v(\epsilon, t) = \frac{\Delta r(t)}{t}$. In Fig.5(d), we show the variation of the normalized effective transport speed $\frac{v(\epsilon, t)}{v_0}$ for four values of disorder strengths ϵ ($= 0, 1, 1.5$ and 2). We note that $\frac{v(\epsilon, t)}{v_0}$ decreases with increasing strength of the disorder. Hence, we claim that due to random nature of different interaction strength, dynamics of the particle become slow for high disorder strength. It further leads to strong clustering on increasing the strength of disorder.

B. Dynamical Behaviour

Ordering kinetics to the steady state

In previous sections, we have discussed the steady-state properties of the ordered state. In this sec-

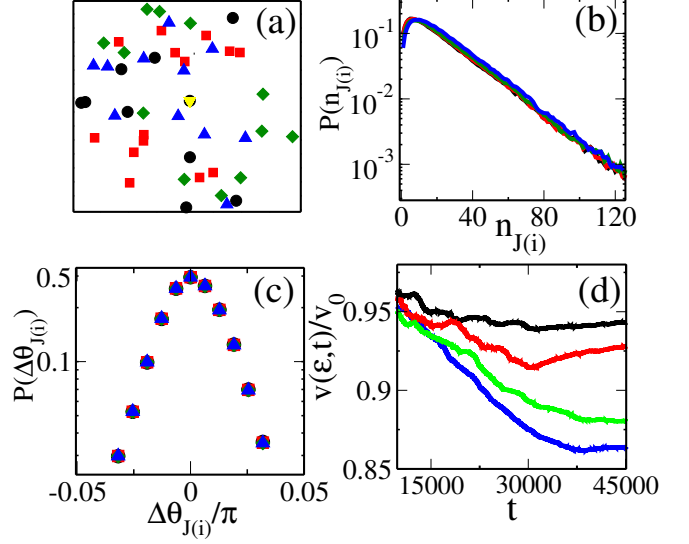


FIG. 5. (color online) (a) Snapshot of the neighbour particles within the interaction radius ($R = 1.0$) of a tagged particle in the steady state for disorder strength $\epsilon = 2.0$. $N = 10000$. The filled black circles, red squares, green diamonds, and blue triangles denote $0 \leq J < 0.5$, $0.5 \leq J < 1.0$, $1.0 \leq J < 1.5$, and $1.5 \leq J \leq 2.0$, respectively. At the centre of the box, yellow triangle indicates the tagged particle. (b,c) Plots of $P(n_{J(i)})$ and $P(\Delta\theta_{J(i)})$ distribution for different $J(i)$ ranges, respectively. $N = 62500$. Color lines and symbols in (b,c) indicate same things as in (a). (d) Plot of normalise effective transport speed $v(\epsilon, t)/v_0$ vs. t . Black, red, green and blue lines represent $\epsilon = 0.0, 1.0, 1.5$ and 2 respectively. $N = 10000$.

tion, we discuss the effects of the random-bond disorder on the ordering kinetics when the system is quenched from a random disordered state to an ordered steady state. Kinetics of the orientation ordering is characterised by calculating the two-point orientation correlation function $C(r, t) = \frac{\langle \sum_{ij} \mathbf{n}_i(\mathbf{r}_0, t) \cdot \mathbf{n}_j(\mathbf{r} + \mathbf{r}_0, t) \rangle - \frac{\sum_{ij} \langle \mathbf{n}_i(\mathbf{r}_0, t) \rangle \langle \mathbf{n}_j(\mathbf{r} + \mathbf{r}_0, t) \rangle}{N(N-1)}}{N(N-1)}$, where second term on the right hand side is zero. $\langle \dots \rangle$ represents average over many reference points r_0 's and 10 independent realizations. We note that $C(r, t)$ grows with time for all disorder strengths ϵ as shown in inset of Fig.6(a),(b). In the main plot of Fig.6 (a) and (b), we find nice scaling with respect to the reduced length $r/L_o(t)$, where $L_o(t)$ is the characteristic domain size and it is obtained from the first 0.17 crossing of the correlation function $C(r, t)$. The plot of $L_o(t)$ vs. time t for the clean system $\epsilon = 0$ and for the RBDPF ($\epsilon = 1, 2$) are shown in Fig.6(c). We note that the disorder has no effect on the kinetics of growing domains. Moreover, the size of domains varies as, $L_o(t) \simeq t^{1/z_o}$ with $z_o \sim 2$ for all disorder strengths. We also calculate the kinetics of the growth of the density cluster. Density growth is measured by the mass of the largest cluster $m(t)$. The mass of the largest cluster $m(t)$ is calculated using the cluster counting algorithm [53]. The plot of $m(t)$ vs. time t for the clean system $\epsilon = 0$ and the RBDPF, $\epsilon = 1, 2$, are shown in Fig. 6(d). For all

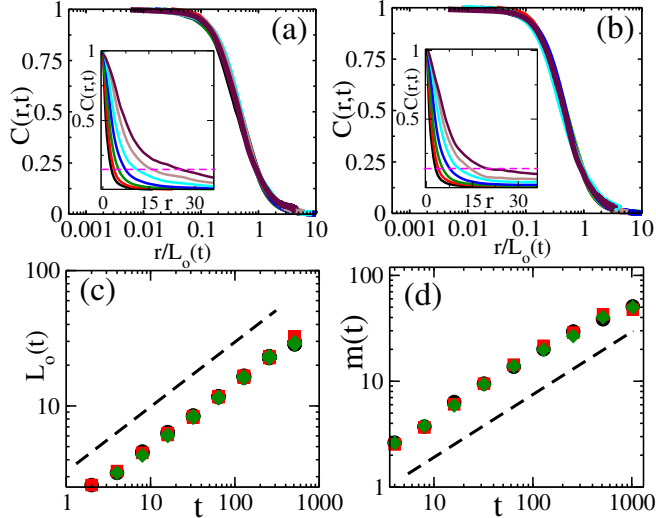


FIG. 6. (color online) (a,b) Plots $C(r,t)$ vs. r/L_o for $\epsilon = 0$ and 2, respectively in semi-log Y-scale. Black, red, green, blue, cyan, brown and violet lines represents time $t = 2, 4, 16, 32, 64, 128$ and 256, respectively. In the *inset* of (a) and (b), the variation $C(r,t)$ with r is shown at different time. Different colored lines represent same thing as the main figure. Dashed line with color magenta is drawn parallel to x-axis and intersect y-axis at 0.17 (crossing point) . $N = 262144$ (c) Plot of $L_o(t)$ with time t in log – log scale. The dashed line represents the slope 0.5. $N = 262144$. (d) Plot of mass of the largest cluster $m(t)$ with time t in log – log scale. $N = 40000$. The dashed line represents the slope 0.5. The filled black circles, red squares, and green diamonds represent $\epsilon = 0.0, 1.0$ and 2.0, respectively.

cases, $m(t)$ grows with time as t^α with $\alpha \sim 0.5$. Hence, the length of the density cluster $L_\rho(t) \simeq \sqrt{m(t)} \sim t^{1/z_\rho}$ and $z_\rho \sim 4$, which is similar to the asymptotic growth exponent for the conserved field in the active model B [50, 51].

IV. DISCUSSION

We introduced a minimal model of a collection of self-propelled particles with the random-bond disorder. Each particle has a different ability (interaction strength) to influence its neighbours. The varying interaction strength is obtained from a uniform distribution and it can be varied from $[1 - \epsilon/2 : 1 + \epsilon/2]$, where ϵ is the disorder strength. For $\epsilon = 0$, the model reduces to the uniform interaction strength model or the Vicsek-like model [8]. The equilibrium analogue of the present model is the random-bond XY model. We studied the characteristics of the ordered steady state for different strengths of the disorder. The random-bond disorder does not affect the usual LRO present in a clean polar

flock. To our surprise, the random-bond disorder leads to a more cohesive flock, hence, more inhomogeneous or dense clusters. This phenomenon is due to the slower dynamics of a particle moving in a random network of different interaction strengths. Although the disorder affects the local density inhomogeneity, the global density fluctuation remains unaffected and the system shows the usual giant number fluctuation (GNF).

Furthermore, we also studied the effects of the random-bond disorder on the ordering kinetics of the orientation and the density fields. We note that the orientation field in a polar flock with uniform interaction coarsens with time with a growth exponent $z_o \sim 2$ whereas the growth exponent for the density field $z_\rho \sim 4$. Moreover, the coarsening for both the fields remain unaffected in the presence of random-bond disorder as opposed to what is observed in the corresponding equilibrium model [46, 47]. Hence, our study introduces the effect of the random-bond disorder in a polar flock and shows many interesting features that are in general not present in the corresponding equilibrium system with random-bond disorder [46, 47]. Our study provides a new direction to understand the effects of intrinsic inhomogeneity in many natural active systems.

V. ACKNOWLEDGEMENT

J. P. Singh thanks computational facility at IIT(BHU), Varanasi. S. Pattanayak thanks TUE computational facility at S.N.B.N.C.B.S. S. Mishra thanks Department of Science and Technology, Science and Engineering Research Board (India), project no. ECR/2017/000659 for partial financial support.

Appendix A: Linearised study of hydrodynamic equations of motion

We define local density of the particles as,

$$\rho(\mathbf{r}, t) = \sum_{i=1}^N \delta(\mathbf{r} - \mathbf{R}_i(t)) \quad (\text{A1})$$

where, \mathbf{R}_i and N are the position vector of the i^{th} particle and total number of particles respectively. Similarly we define the local polarisation density field as

$$\mathbf{P}(\mathbf{r}, t)\rho = \sum_{i=1}^N \mathbf{n}_i(t)\delta(\mathbf{r} - \mathbf{R}_i(t)). \quad (\text{A2})$$

We can write the coupled hydrodynamic equations of motion for density and polarization fields as obtained in the study [14, 15, 17].

$$\partial_t \rho = -v_0 \nabla \cdot (\mathbf{P} \rho) \quad (\text{A3})$$

$$\partial_t \mathbf{P} = \left(\alpha_1(\rho, \epsilon) - \alpha_2 \mathbf{P} \cdot \mathbf{P} \right) \mathbf{P} - \frac{v_1}{2\rho_0} \nabla(\rho) + \lambda(\mathbf{P} \cdot \nabla) \mathbf{P} + D_p \nabla^2 \rho + \mathbf{f}_p(\mathbf{r}, t) \quad (\text{A4})$$

For the random-bond disorder model, we introduce an additional general ϵ dependence term to alignment parameter α_1 in the Eq.((A4)). α_1 is considered as a constant in the study by Toner *et al.* [14] whereas have density and noise dependence in [15, 17]. Here we show in steps, how we get the specific depdence of α_1 on ϵ . Starting from the position and orientation update (without repulsion) as given in Eq.((A1)) and ((A2)), we can write

$$\partial_t(\mathbf{P} \rho) = \frac{\sum_i [\mathbf{n}_i(t + \Delta t) \delta(\mathbf{r} - \mathbf{R}_i(t + \Delta t)) - \mathbf{n}_i(t) \delta(\mathbf{r} - \mathbf{R}_i(t))]}{\Delta t} \quad (\text{A5})$$

The above discretisation of time derivative are written by approximating all the relevant time scales are much larger than the unit time step of updation. $\mathbf{n}_i(t + \Delta t)$ and $\mathbf{R}_i(t + \Delta t)$ is obtained from the two upadtes of orientation and poistion as given in Eq.((1)) and ((2)) and we have taken $\Delta t = 1.0$ in the simulation. After substitution of the orientation and position at time $t + \Delta t$, we find

$$\partial_t(\mathbf{P} \rho) = \sum_i \frac{[\sum_j J_j \mathbf{n}_j + N_i \phi_i \eta] [\delta(\mathbf{r} - \mathbf{R}_i(t) - v_0 \mathbf{n}_i(t))]}{\omega_i} - \sum_i [\mathbf{n}_i(t) \delta(\mathbf{r} - \mathbf{R}_i(t))] \quad (\text{A6})$$

where $\omega_i = \|\sum_j \mathbf{n}_j(t) + N_i \phi_i \eta\|$, where $\|\cdot\|$ means norm of the vector inside. After using the distribution $P(J_j)$ from the uniform distribution of J_j from $[1 - \epsilon/2 : 1 + \epsilon/2]$ and use this in the summation inside the interaction radius and replacing it the summation by the integral (since the distribution of J is continuous), we find that the first term (linear term in \mathbf{P}) in Eq. ((A4)) will be of the form $\alpha_1(\rho, \epsilon) = \alpha_0 \left(\rho_0 \left(\frac{1+\epsilon^2/12}{1-\epsilon^2/84} \right) - \eta^2 \right)$, where α_0 is a constant.

Another derivation of the hydrodynamic equations from the microscopic update equation is similar to as given in [16, 20]. For simplicity, we assume all other terms are independent of the disorder.

Eq.((A3)) represents continuity equation for the conserved density field ρ with a flux controlled by, $-v_0 \nabla \cdot (\mathbf{P} \rho)$ describes convection due to self-propulsion speed $v_0 \mathbf{P}$. In Eq.((A4)), the first term on right hand side represents a mean field transition from an isotropic state ($\mathbf{P} = 0$) to a broken symmetry state $\mathbf{P} = \sqrt{\frac{\alpha_1(\rho_0, \epsilon)}{\alpha_2}} \hat{\mathbf{x}}$ (the direction of broken symmetry is chosen along x -axis). The second and third term indicate hydrostatic pressure due to density gradient and convection in the model, respectively. Both λ and v_1 depends on self-propelled speed of the particle [15]. Here in present study we assume it $\sim v_0$. The fourth term represents diffusion in the polarisation field. The last term is noise in the system $\mathbf{f}_p(\mathbf{r}, t) = (f_{p_x}(\mathbf{r}, t), f_{p_y}(\mathbf{r}, t))$ is white Gaussian white noise with mean zero and variance Δ_p . We perturb the system about the homogeneous steady state solution of Eqs. ((A3)) and ((A4)) and write $\rho(\mathbf{r}, t) = \rho_0 + \delta\rho$ and $\mathbf{P}(\mathbf{r}, t) = (p_0 + \delta p_x(t)) \hat{\mathbf{x}} + (\delta p_y(t)) \hat{\mathbf{y}}$, where $p_0(t) = \sqrt{\frac{\alpha_1(\rho_0, \epsilon)}{\alpha_2}}$. We write the linearised hydrodynamic equations for small perturbations in three fields $\delta\rho(t)$, $\delta p_x(t)$ and $\delta p_y(t)$ as,

$$\partial_t \delta p_x = \left(\alpha'_1(p_0) p_0 - \frac{v_1}{2\rho_0} \partial_x \right) \delta\rho - 2\alpha_1(\rho_0, \epsilon) \delta p_x \quad (\text{A7})$$

$$\partial_t \delta p_y(t) = \lambda p_0 \partial_x \delta p_y + D_p \nabla^2 \delta p_y - \frac{v_1}{2\rho_0} \partial_y \delta\rho + f_{p_y}(\mathbf{r}, t), \quad (\text{A8})$$

$$\partial_t \delta\rho(t) = -v_0 (\partial_x (p_0 + \delta p_x) (\rho_0 + \delta\rho) + \partial_y \delta p_y (\rho_0 + \delta\rho)) \quad (\text{A9})$$

where δp_x and δp_y are in the directions of broken symmetry and perpendicular to it, respectively and $\alpha'_1 = \frac{\partial \alpha_1(\rho)}{\partial \rho} |_{\rho_0} = \alpha_0 \frac{(1+\epsilon^2/12)}{(1-\epsilon^2/84)}$. In writing Eq.((A7)), we assumed that fluctuations in the longitudinal direction is long range and higher order derivatives are negligible. In the steady state, using Eq.((A7)) we can solve for δp_x

$$\delta p_x = \frac{(\alpha'_1 p_0 - \frac{v_1}{2\rho_0} \partial_x) \delta\rho}{2\alpha_1(\rho_0, \epsilon)}. \quad (\text{A10})$$

We substitute δp_x from Eq.((A10)) in Eqs. ((A8)) and ((A9)) and write effective dynamical equations for δp_y and $\delta \rho$ as,

$$\partial_t \delta p_y = \lambda p_0 \partial_x \delta p_y + D_p \nabla^2 p_y - \frac{v_1}{2\rho_0} \partial_y \delta \rho \quad (\text{A11})$$

$$\partial_t \delta \rho = v_0 p_0 V_x \partial_x \delta \rho + D_\rho \partial_x^2 \delta \rho - v_0 \rho_0 \partial_y \delta p_y \quad (\text{A12})$$

where, $V_x = (\frac{\rho_0 \alpha_1'}{2\alpha_1} + 1)$, $D_\rho = \frac{v_0 v_1}{4\alpha_1}$ and $\alpha_1 = \alpha_1(\rho_0, \epsilon)$. Furthermore, we take the Fourier transform of Eq.((A11)) and ((A12)) using $Y(\mathbf{r}, t) = \int d\mathbf{k} \exp(-i(\mathbf{k} \cdot \mathbf{r} + \omega t)) Y(\mathbf{k}, \omega)$ and write different terms in matrix notation,

$$M \begin{bmatrix} \delta \rho \\ \delta p_y \end{bmatrix} = \begin{bmatrix} 0 \\ f_{p_y} \end{bmatrix} \quad (\text{A13})$$

where, the coefficient matrix M can be written as,

$$M = \begin{bmatrix} (-i\omega + iq_x v_0 p_0 V_x - D_\rho q_x^2) & (-v_0 \rho_0 iq_y \delta p_y) \\ (\frac{iv_1}{2\rho_0} q_y \delta \rho) & (-i\omega - \lambda p_0 iq_x - D_p q^2) \end{bmatrix}. \quad (\text{A14})$$

The Eq.((A14)) gives the two modes from the linearised hydrodynamics calculations,

$$\omega_\pm = C_\pm(\theta)q - i\Gamma_L \left[\frac{V_\pm(\theta)}{2C_2(\theta)} \right] - i\Gamma_\rho \left[\frac{V_\pm(\theta)}{2C_2(\theta)} \right], \quad (\text{A15})$$

where, $C_\pm(\theta) = \frac{\gamma + v_0 V_x}{2} \cos \theta \pm C_2(\theta)$, $C_2(\theta) = \sqrt{\frac{(\gamma - v_0 V_x)^2 \cos^2 \theta}{4} + \rho_0 v_1 \sin^2 \theta}$, $\gamma = -\lambda v_0$, $\Gamma_\rho(q) = D_\rho q_x^2$, $\Gamma_L(q) = D_p q^2$ and $V_\pm(\theta) = C_2(\theta) \pm \frac{\gamma - v_0 V_x}{2} \cos \theta$. θ is the angle between flock direction and propagation vector \mathbf{q} , and $\Gamma_\rho(q)$ and $\Gamma_L(q)$ are the wave vectors dependent on damping. Using Eq.((A13)) we get

$$\begin{bmatrix} \delta \rho \\ \delta p_y \end{bmatrix} = M^{-1} \begin{bmatrix} 0 \\ f_{p_y} \end{bmatrix} \quad (\text{A16})$$

Therefore, solution for the fluctuations in ρ , $\delta \rho(q, \omega) = G_{\rho p}(q, \omega) f_{p_y}(\mathbf{q}, \omega)$, where the propagator $G_{\rho p}(q, \omega)$ can be written as,

$$G_{\rho p}(q, \omega) = \frac{v_0 \rho_0 iq_y}{(\omega - C_+(\theta)q)(\omega - C_-(\theta)q) + [i\omega(\Gamma_\rho(q) + \Gamma_L(q)) - iq \cos \theta (\gamma \Gamma_\rho(q) + v_0 V_x \Gamma_L(q))]} \quad (\text{A17})$$

Furthermore, the two-point density-density correlation function, $C_{\rho\rho} = \langle |\delta \rho(q, \omega)|^2 \rangle$, can be written as,

$$C_{\rho\rho} = \frac{v_0^2 \rho_0^2 q_y^2 \Delta_p}{(\omega - C_+(\theta)q)^2 (\omega - C_-(\theta)q)^2 + [\omega(\Gamma_\rho(q) + \Gamma_L(q)) - q \cos \theta (\gamma \Gamma_\rho(q) + v_0 V_x \Gamma_L(q))]^2} \quad (\text{A18})$$

Moreover, the density fluctuation $\langle |\delta \rho(\mathbf{q}, \omega)| \rangle$ can be obtained as,

$$\sqrt{C_{\rho\rho}} = \left[\frac{v_0 \rho_0 \sin \theta \sqrt{\Delta_p}}{C_+(\theta)(\Gamma_\rho + \Gamma_L) - \cos \theta (\gamma \Gamma_\rho + v_0 V_x \Gamma_L)} \right] + \left[\frac{v_0 \rho_0 \sin \theta \sqrt{\Delta_p}}{C_-(\theta)(\Gamma_\rho + \Gamma_L) - \cos \theta (\gamma \Gamma_\rho + v_0 V_x \Gamma_L)} \right]. \quad (\text{A19})$$

We can write Eq.((A19)) in a simple form for fluctuation in $\theta = \pi/4$ and for finite $q \sim 1$,

$$\langle |\delta \rho| \rangle = \sqrt{\Delta_p} \left[\frac{(C_+(\theta)D_\rho - A) + (C_-(\theta)D_\rho - A)}{(C_+(\theta)D_\rho - A)(C_-(\theta)D_\rho - A)} \right]. \quad (\text{A20})$$

Substituting $A = \gamma D_\rho + v_0 V_x \Gamma_L$, $C_+ + C_- = \frac{\gamma + v_0 V_x}{2}$, $C_+ C_- = \gamma v_0 V_x$ in Eq.((A20)) and further simplification gives,

$$\langle |\delta \rho| \rangle = \frac{\rho_0 \sqrt{\Delta_p} \alpha_0 \left(\rho_0 \frac{1+\epsilon^2/12}{1-\epsilon^2/84} - \eta^2 \right)}{\gamma v_1 + \rho_0 \alpha_0 \left(\frac{1+\epsilon^2/12}{1-\epsilon^2/84} \right) + 1}. \quad (\text{A21})$$

Substituting value of $\epsilon = [0.0, 2.0]$, $v_0 = 0.5$, $\eta = 0.2$ and $\Delta_p = 0.1$ and using α_0 as fitting parameter to match the curve for smallest $\rho_0 = 0.5$ we found $\alpha_0 = 8$, curve matches well. Then changed value of $\rho_0 = 1.0$ and 2.0 for other two curves. The γ and $v_1 \sim v_0$. The plot of $\langle |\delta \rho| \rangle$ for three ρ_0 is shown by the dashed line in Fig.4(c).

- [2] H. Yokota (private communication); Y. Harada, A. Noguchi, A. Kishino, and T. Yanagida, *Nature (London)* **326**, 805 (1987); Y. Toyoshima et al., *Nature (London)* **328**, 536 (1987); S. J. Kron and J. A. Spudich, *Proc. Natl. Acad. Sci. U.S.A.* **83**, 6272 (1986).
- [3] S. Garcia, E. Hannezo, J. Elgeti et. al. *PNAS* **112** (50) 15314-15319 (2015).
- [4] J. T. Bonner, *Proc. Natl. Acad. Sci. U.S.A.* **95**, 9355 (1998); M. T. Laub and W. F. Loomis, *Mol. Biol. Cell* **9**, 3521 (1998).
- [5] D. Chen, Y. Wang, G. Wu, M. Kang, Y. Sun, and W. Yu, *Chaos* **29**, 113118 (2019).
- [6] *Three Dimensional Animals Groups*, edited by J. K. Parrish and W. M. Hamner (Cambridge University Press, Cambridge, England, 1997).
- [7] D. Helbing, I. Farkas, and T. Vicsek, *Nature (London)* **407**, 487 (2000).
- [8] T. Vicsek, A. Czirók, E. Ben-Jacob, I. Cohen, and O. Shochet, *Phys. Rev. Lett.* **75**, 1226 (1995).
- [9] Lucas Barberis *Phys. Rev. E* **98**, 032607 (2018)
- [10] J.P Singh. Sameer Kumar and Shradha Mishra (to be published).
- [11] D Geyer, D Martin, J Tailleur, D Bartolo. *Physical Review X* **9** (3), 031043, (2019).
- [12] N Sepúlveda, L Petitjean, O Cochet, E Grasland-Mongrain, P Silberzan et. al. *PLoS Comput Biol* **9** (3), e1002944, (2013).
- [13] L Caprini, UMB Marconi, A Puglisi. *Phys. Rev. Lett.* **124** (7), 078001, (2020).
- [14] J. Toner and Y. Tu, *Phys. Rev. E* **58**, 4828 (1998).
- [15] E. Bertin et al., *Phys. Rev. E* **74**, 022101 (2006)
- [16] E Bertin, H Chaté, F Ginelli, S Mishra, A Peshkov, S Ramaswamy *New J. Phys.* **15** (8), 085032
- [17] T. Ihle, *Phys. Rev. E* **83**, 030901 (2011),
- [18] G. Grégoire and H. Chaté, *Phys. Rev. Lett.* **92**, 025702 (2004).
- [19] H. Chaté, F. Ginelli, Guillaume Grégoire, and F. Raynaud, *Phys. Rev. E* **77**, 046113 (2008).
- [20] S. Pattanayak and S. Mishra, *J. Phys. Commun.* **2**, 045007 (2018).
- [21] M. Romensky, V. Lobaskin, and T. Ihle, *Phys. Rev. E* **90**, 063315 (2014).
- [22] A. Morin, N. Desreumaux, J. Caussin, and D. Bartolo, *Nature Physics* **13**, 63–67 (2017).
- [23] O. Chepizhko, E. G. Altmann, and F. Peruani, *Phys. Rev. Lett.* **110**, 238101 (2013).
- [24] D. Yllanes, M. Leoni, and M. C. Marchetti, *New J. Phys.* **19**, 103026 (2017).
- [25] D. A. Quint and A. Gopinathan, *Phys. Biol.* **12**, 046008 (2015).
- [26] C. Sándor, A. Libál, C. Reichhardt, and C. J. Olson Reichhardt, *Phys. Rev. E* **95**, 032606 (2017).
- [27] C. J. O. Reichhardt and C. Reichhardt, *Nat. Phys.* **13**, 10 (2017).
- [28] R. Das, M. Kumar, and S. Mishra, *Phys. R. E.* **98**, 060602(R) (2018).
- [29] J. Toner, N. Guttenberg, and Y. Tu, *Phys. Rev. E* **98**, 062604 (2018).
- [30] J. Toner, N. Guttenberg, and Y. Tu, *Phys. Rev. Lett.* **121**, 248002 (2018).
- [31] R. Das, M. Kumar, and S. Mishra, *Phys. Rev. E* **101**, 012607 (2020).
- [32] S. Pattanayak, J. P. Singh, M. Kumar, and S. Mishra, *Phys. Rev. E* **101**, 052602 (2020).
- [33] Guo-yuan Wang, Fan-yu Wu, You-liang Si, Q. Zeng, and P. Lin, *Procedia Engineering* **211**, 699 (2018).
- [34] G. A. Frank and C. O. Dorso, *Physica A (Amsterdam, Neth.)* **390**, 2135 (2011).
- [35] A. Garcimartín, D. R. Parisi, J. M. Pastor, C. Martín-Gómez, and I. Zuriguel, *J. Stat. Mech.* **4**, 043402 (2016).
- [36] I. Zuriguel, J. Olivares, J. M. Pastor, C. Martín-Gómez, L. M. Ferrer, J. J. Ramos, and A. Garcimartín, *Phys. Rev. E* **94**, 032302 (2016).
- [37] I. Zuriguel, A. Janda, A. Garcimartín, C. Lozano, R. Arévalo, and D. Maza *Phys. Rev. Lett.* **107**, 278001 (2011).
- [38] V. L. Berezinskii, *JETP* **32**, 493 (1971).
- [39] J. M. Kosterlitz and D. J. Thouless, *J. Phys. C* **6**, 1181 (1973).
- [40] J. M. Kosterlitz, *J. Phys. C* **7**, 1046 (1974).
- [41] S. Puri and C. Roland, *Phys. Lett. A* **151**, 500 (1990).
- [42] S. Puri, *Phys. Lett. A* **164**, 211 (1992).
- [43] S. Puri, D. Chowdhury, and N. Parekh, *J. Phys. A* **24**, L1087 (1991).
- [44] W. Bialek, A. Cavagna, I. Giardina, T. Mora, E. Silvestri, M. Viale, and A. M. Walczak, *PNAS* **109**, 4786 (2012).
- [45] Vik. S. Dotsenko and M. V. FeTgel'man, *Zh. Eksp. Teor. Fiz.* **83**, 345 (1982).
- [46] M. Kumar, S. Chatterjee, R. Paul, and S. Puri, *Phys. Rev. E* **96**, 042127 (2017).
- [47] D. J. Bishop and J. D. Reppy, *Phys. Rev. Lett.* **40**, 1727(1978).
- [48] A. J. Bray, *Advances in Physics* **43**, 357 (1994).
- [49] S. Puri, and V. Wadhawan, *Kinetics of Phase Transitions*, CRC press (2009).
- [50] R. Wittkowski, A. Tiribocchi, J. Stenhammar, R. J. Allen, D. Marenduzzo, and M. E. Cates, *Nature Communications* **5**, 4351 (2014).
- [51] S. Pattanayak, S. Mishra, and S. Puri (to be published).
- [52] B. Bhattacharjee, S. Mishra, S.S. Manna, *Phys. Rev. E.* **92**, 062134 (2015).
- [53] C. P. Beatrice, R. M. C. de Almeida, and L. G. Brunnet, *Phys. Rev. E.* **95**, 032402 (2017).